Star Clusters: From the Milky Way to the Early Universe
Proceedings IAU Symposium No. 351, 2019
A. Bragaglia, M. Davies, A. Sills & E. Vesperini, eds.

doi:10.1017/S1743921319007208

Globular cluster system of NGC 3613, a massive elliptical galaxy in a poor environment

Bruno J. De Bórtoli[1,2], Lilia P. Bassino[1,2], Juan P. Caso[1,2] and Ana I. Ennis[1,2]

[1]Facultad de Ciencias Astronómicas y Geofísicas de la Universidad Nacional de La Plata, and Instituto de Astrofísica de La Plata (CCT La Plata – CONICET, UNLP), Paseo del Bosque S/N, B1900FWA La Plata, Argentina

[2]Consejo Nacional de Investigaciones Científicas y Técnicas, Godoy Cruz 2290, C1425FQB, Ciudad Autónoma de Buenos Aires, Argentina

Abstract. We present an analysis of the globular cluster system (GCS) of the galaxy NGC 3613, an intrinsically bright elliptical galaxy ($M_V = -21.5$) in a low density environment (it is the central galaxy of a group of a dozen galaxies). Based on Gemini/GMOS photometry of NGC 3613 we obtained the following properties for this GCS. A 'blue tilt' is detected in the colour-magnitude diagram. The colour distribution is bimodal, presenting the two classical globular cluster (GC) sub-populations. The spatial and azimuthal projected distributions show that red sub-population correlates with the stellar component of the host galaxy.

Keywords. galaxies: clusters: individual: NGC 3613 – galaxies: elliptical and lenticular, cD – galaxies: evolution.

1. Introduction

Globular clusters (GCs) are among the oldest objects in the Universe. They originated in massive star formation events, such as those that occur when two galaxies merge, in conditions of high density and pressure (Kruijssen 2014). According to numerical simulations like the E-MOSAICS Project (Pfeffer *et al.* 2018; Kruijssen *et al.* 2019), there is a direct correlation between the formation of GCs and the field stars. Then, the analysis of the properties of a globular cluster system (GCS) associated to a galaxy provides clues about its formation and evolution.

In particular, our target, NGC 3613 is an intrinsically bright elliptical galaxy ($M_V = -21.5$) located in a low density environment (a group of a dozen galaxies). de Vaucouleurs *et al.* (1991) classified it as E6 and according to Tully *et al.* (2013), based on surface brightness fluctuations, it has a distance of d$\sim$ 30.1 Mpc.

Located at 47 arcmin towards the north, there is a lenticular galaxy of similar luminosity, NGC 3610, that has a surface brightness distribution with plumes, tails and other structures as a consequence of the tidal disturbances suffered during its evolution (Schweizer & Seitzer 1992; Bassino & Caso 2017). Madore *et al.* (2004) indicate that both galaxies are part of the same group. One of the aims of this work is to study possible interactions between NGC 3613 and NGC 3610.

This proceeding is organized as follows. The observations and data reduction are described in Section 2, while the results are presented in Section 3.

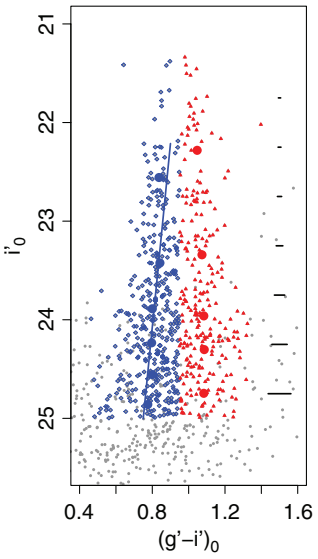

Figure 1. Colour-magnitude diagram for the point sources (highlighted triangles and rhombuses show metal-rich (red) and metal-poor (blue) GC candidates respectively). Large dots represent colour averages of different subsamples, sorted in magnitude, with equal number of GC candidates.

2. Observations and data reduction

The data consist of images obtained with Gemini/GMOS-N during semester 2013A (programme GN2013A-Q-42, PI: J.P. Caso) in g', r', and i'-bands. On the one hand, one field centred on the galaxy NGC 3610 plus another 'adjacent' field were taken and have been the basis to study this galaxy (Bassino & Caso 2017). On the other hand, one field on the galaxy NGC 3613 was taken as part of the same programme and was used in the present study. In order to estimate the contamination by Galactic stars and background galaxies, we used the 'adjacent field'.

For the data reduction, tasks of the gemini package (in particular, GMOS package) and IRAF DAOPHOT were used. We performed PSF photometry and estimated the photometric completeness for our fields.

3. Results

3.1. *Colour-magnitude diagram and blue tilt*

Fig. 1 shows the colour-magnitude diagram i'_0 versus $(g'-i')_0$ for point sources in our science field. They were selected by colour and magnitude and are shown with triangles and rhombuses for metal-rich (red) and metal-poor (blue) GC candidates respectively. Large dots represent colour averages of different subsamples, sorted in magnitude, with equal number of candidates. We can see that as we consider brighter blue GC candidates, they get redder. This effect is known as "blue tilt". It was initially considered as a mass-metallicity relationship, in a way that more massive GCs became redder by a process of self-enrichment (Bailin & Harris 2009). Then Usher *et al.* (2018) suggested that the slope is due to a deficiency of the bluer and brighter GCs of the blue sub-population. Recently, Choksi & Gnedin (2019) proposed that a cut in the cluster initial mass function, usually represented by a power law, would be responsible for this slope observed in the colour-magnitude diagram.

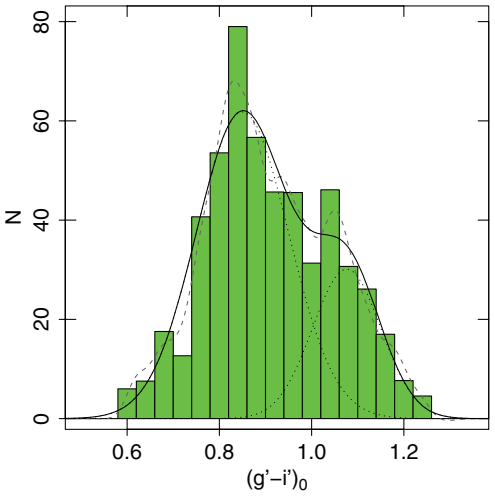

Figure 2. Colour distribution of the selected GCs. Dotted lines represent the resulting Gaussian fit for each sub-population, and the solid one shows their sum. The dashed curve corresponds to a smoothed distribution.

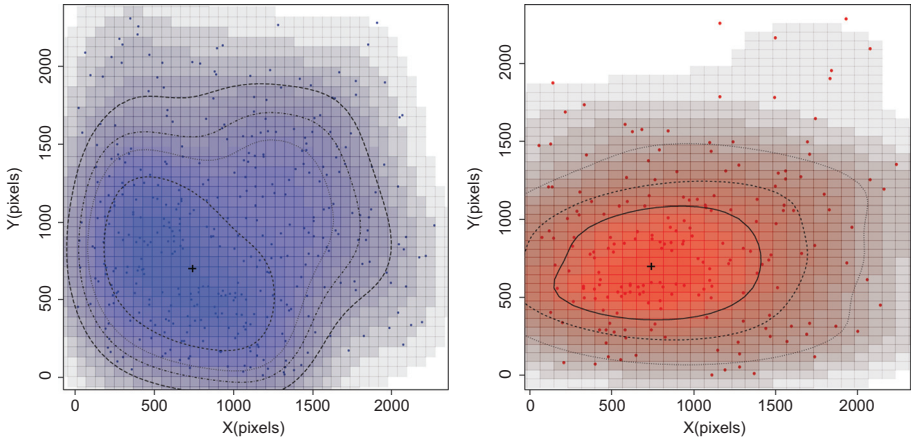

Figure 3. Projected spatial distribution for GC sub-populations in the left and right panels, respectively.

3.2. *Colour distribution*

Fig. 2 shows the colour distribution. Two Gaussians were fitted with GMM (Muratov & Gnedin 2010). Dotted lines represent the resulting Gaussian fit for each sub-population, and the solid one shows their sum. The dashed curve corresponds to a smoothed distribution. A classic scenario is observed here, where we can see two sub-populations with the typical mean colours $(g' - i')_0 = 0.85$ and $(g' - i')_0 = 1.07$ (e.g. Harris *et al.* 2009).

3.3. *Projected spatial distribution*

Fig. 3 shows the projected spatial distribution of the GC candidates. The red GC sub-population is more concentrated towards the centre of the galaxy and with elliptical contours, while the blue sub-population is more extended and with contours presenting no

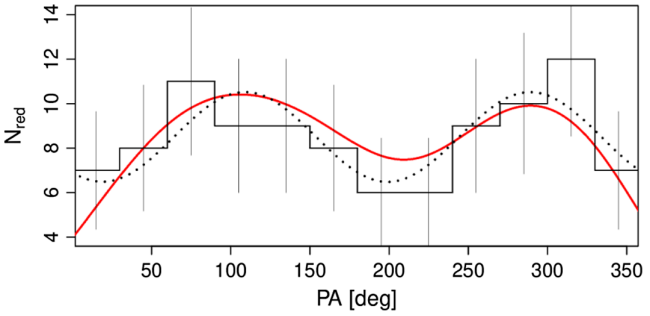

Figure 4. Azimuthal projected distribution of red GC sub-population. Dotted and solid lines show the fit and the smoothed histograms, respectively.

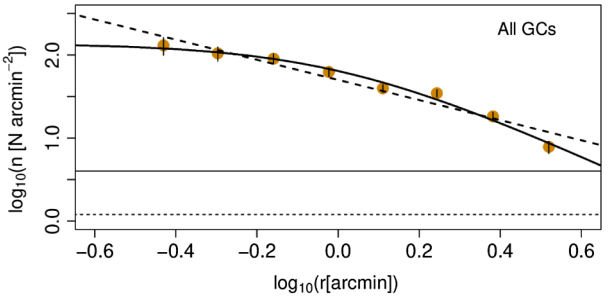

Figure 5. Radial GC projected distribution. Solid and dashed lines show fits using a Hubble profile and a power-law, respectively. The solid and dotted horizontal lines represent the value of the background level and its 30 percent respectively.

clear shape. The major axis and ellipticities of red contours are similar to the equivalent of the galaxy surface-brightness distribution.

3.4. *Azimuthal projected distribution*

Fig. 4 shows the azimuthal projected distribution of the red GC sub-population. The dotted line shows a fitted sinusoidal function, which corresponds to an elliptical projected distribution similar to the galaxy surface-brightness distribution. The solid line shows the smoothed histogram.

3.5. *Radial projected distribution*

Fig. 5 shows the radial projected distribution for all GC candidates corrected by background contamination and by completeness. Solid and dashed lines show fits using a Hubble profile and a power-law, respectively. The solid and dotted horizontal lines represent the value of the background level and its 30 percent respectively. The later value is used to estimate the extension of the GCS, for wich we obtained r = 72 kpc.

References

Bailin, J. & Harris, W. E. 2009, *APJ*, 695, 1082
Bassino, L. P. & Caso, J. P. 2017, *MNRAS*, 466, 4259
Choksi, N. & Gnedin, O. Y. 2019, *MNRAS*, 695, 1082
de Vaucouleurs, G., de Vaucouleurs, A., Corwin, Jr.H. G., Buta, R. J., Paturel, G., & Fouqué, P. 1991, *Third Reference Catalogue of Bright Galaxies.*,
Harris, W. E., Kavelaars, J. J., Hanes, D. A., Pritchet, C. J., & Baum, W. A. 2009, *AJ*, 137, 3314

Kruijssen, J. M. D. 2014, *Classical and Quantum Gravity*, 31, 24
Kruijssen, J. M. D., Pfeffer, J. L., Crain, R. A., & Bastian, N. 2014, *MNRAS*, 486, 3
Madore, B. F., Freedman, W. L., & Bothun, G. D. 2004, *APJ*, 607, 810
Muratov, A. L. & Gnedin, O. Y. 2010, *APJ*, 718, 1266
Pfeffer, J. L., Kruijssen, J. M. D., Crain, R. A., & Bastian, N. 2018, *MNRAS*, 475, 4
Schweizer, F. & Seitzer, P. 1992, *AJ*, 104, 1039
Tully, R. B, Courtois, H. M., Dolphin, A. E., Fisher, J. R., Héraudeau, P., Jacobs, B. A., Karachentsev, I. D., Makarov, D., Makarova, L., Mitronova, S., Rizzi, L., Shaya, E. J., Sorce, J. G., & Wu, P.-F. 2013, *AJ*, 146, 86
Usher, C., Pfeffer, J., Bastian, N., Kruijssen, J. M. D., Crain, R. A., Reina-Campos, M., *et al.* 2018, *MNRAS*, 480, 3279